



ELSEVIER

Contents lists available at ScienceDirect

## Journal of Magnetism and Magnetic Materials

journal homepage: [www.elsevier.com/locate/jmmm](http://www.elsevier.com/locate/jmmm)

## Research articles

## Agglomeration effects in rotating ferrofluids

Sebastian Altmeyer

Castelldefels School of Telecom and Aerospace Engineering, Universitat Politècnica de Catalunya, 08034 Barcelona, Spain

## ARTICLE INFO

## Keywords:

Taylor-Couette flow  
 Ferrofluid  
 Rotating magnetic fluid  
 Bifurcation  
 Agglomeration  
 Elongational flow  
 Flow structure modification

## ABSTRACT

We study flow structure modifications due to *agglomeration*, aggregation and chain formation, also known as *elongational flow* effect for the flow of a ferrofluid in the gap between two concentric rotating cylinders. The system is subjected to either transverse, axial and oblique magnetic field. Consider elongational flow the torque is found to increase or decrease with variation of elongational flow parameter. Furthermore the 3D flow structures themselves are modified, e.g. resulting in variation of different energy portions/contents and the angular momentum transport. The detected modifications are explained by the fact that real ferrofluids consist of a suspension of particles with a finite size in an almost ellipsoid shape as well as with particle–particle interactions that tend to form chains of various lengths and also have a tendency to agglomerate. To come close to such realistic situation for ferrofluids, we consider elongational flow effects incorporated by the symmetric part of the velocity gradient field tensor, which can be scaled by a so-called transport coefficient  $\lambda_2$ . The complexity of structures and modifications depend on the magnetic field configuration. In general complex oblique fields result in stronger interactions and modifications.

## 1. Introduction

Since the classical work by Taylor [1] in 1923 the problem of a viscous flow confined between two coaxially rotating cylinders has been given great attention. From these days on this problem has been greatly studied either theoretically and experimentally and a huge and rich variety of patterns (toroidally closed and helical) have been detected, e.g. with increasing the relative velocity of inner cylinder. Exactly this large number of different flows is a very attractive feature of this experiment and has made this problem important.

When describing the hydrodynamics of ferrofluids, it is typically assumed that the particles aggregate to form clusters having the form of chains, and thus hinders the free flow of the fluid and increases the viscosity [2,3]. In this type of structure formation, it is also assumed that the interaction parameter is usually greater than unity [4], and the strength of the grain-grain interaction can be measured in terms of the total momentum of a particle.

First Müller and Liu consider a different type of model equations [5] based on general principles (including either the Debye theory [6] and the effective field theory by Shliomis [7,8] as special cases) for macroscopic ferrofluid dynamics, the magnetization's relaxation equation includes an additional term that is proportional to the product of the magnetization's magnitude and the symmetric part of the velocity gradient tensor, which can describe an *elongational flow* scaled by a so-called *transport coefficient*  $\lambda_2$ . Typically the term  $\lambda_2$  is a material

dependent function [5] of thermodynamic variables such as density, concentration and temperature, but *independent* of shear. Moreover it can be handled as a *reactive transport coefficient* which does not enter the expression for entropy production. First theoretical studies of elongational flows for dilute suspension considering rigid spheroids focused on elongational viscosity [31] and unveiled a closed form solution for the associated diffusion equation.

Numerous studies can be found in literature devoted to magnetic fluids exposed to external which investigate the influence of finite size particle ferrofluids and their reaction under applied magnetic fields. In particular mass and heat flow of ferrofluid have been under special focus. A recent by Hassan et al. [27], consider rotating disk with low oscillating magnetic field provided deeper understanding of these effects based on different nanoparticle shape behavior, sphere, oblate ellipsoid and prolate ellipsoid. Additional the ferro-particles concentration has been proven to be mainly responsible for changes in the physical properties of liquid which distresses the liquid velocity and temperature distribution [28]. Further works [29,30] used a stretching surface with focus on unsteady boundary layer flow of ferromagnetic fluids and heat transfer past the surface.

The present study has been crucially motivated by the recent work of Storozhenko et al. [9] who investigated different concentrations of ferromagnetic particles under a rotating magnetic field. They detected a field driven agglomeration of particles in case of stationary and slow rotating field, which becomes destroyed for faster rotations. The

E-mail address: [sebastian.andreas.altmeyer@upc.edu](mailto:sebastian.andreas.altmeyer@upc.edu).

<https://doi.org/10.1016/j.jmmm.2019.03.068>

Received 19 April 2018; Received in revised form 16 January 2019; Accepted 13 March 2019

Available online 14 March 2019

0304-8853/ © 2019 Elsevier B.V. All rights reserved.

destruction of agglomeration can be seen in a decreasing torque with increasing rotation frequency of the field. In the present work we do not consider a rotating magnetic field, instead we keep the field constant (in three different configuration) and change the rotation speed of the (inner) cylinder instead (Further we consider either outer cylinder at rest and counter-rotating cylinders). Doing so the effects might be smaller but similar and going into the same direction as detected in [9].

With the present work, we aim to investigate the influence of elongational flow effects [10–12], by direct numerical simulations, considering constant applied magnetic fields (axial, transversal, oblique [32,17,3]), and vary either inner cylinder rotation speed and/or transport coefficient  $\lambda_2$ . Main focus is the variation of torque and flow structural behavior under modification of elongated flow, incorporated over the transport coefficient  $\lambda_2$ .

The paper is organized as follow: Following the introduction, Section 2 describes the system and our methods of investigation. There we present the field equations for the magnetization and the velocity field and we describe implications of the presence of the magnetic terms in the generalized Navier-Stokes equations and finally the full ferrohydrodynamical equations of motion. This is followed by Section 3 presenting our main results.

We first discuss the influence of elongational flow onto torque, angular momentum transport and different energy contents, consider the system with outer cylinder at rest. Following we repeat these studies for counter-rotating cylinders before we investigate the modifications of the 3D flow structures itself. Therefore we illustrate various quantities, e.g. energy (content) dependence, and variation of zero-azimuthal velocity with increasing elongational flow. Finally we summarize the main results with a discussion in Section 4.

## 2. System setting and the Navier-Stokes equation

We consider a standard Taylor-Couette system (TCS) (Fig. 1) consisting of two concentric, independently rotating cylinders. Within the gap between the two cylinders there is an incompressible, isothermal, homogeneous, mono-dispersed ferrofluid of kinematic viscosity  $\nu$  and density  $\rho$ . The inner and outer cylinders have radius  $R_i$  and  $R_o$ , and they rotate with the angular velocity  $\omega_i$  and  $\omega_o$ , respectively. Here, we consider periodic boundary conditions in the axial direction with periodicity of length  $\lambda$  and no-slip boundary conditions on the cylinders. The system can be characterized in the cylindrical coordinate system  $(r, \theta, z)$  by the velocity field  $\mathbf{u} = (u, v, w)$  and the corresponding vorticity field  $\nabla \times \mathbf{u} = (\xi, \eta, \zeta)$ . The radius ratio of the cylinders,  $R_i/R_o$  is kept fixed at 0.5 and the axial periodicity length (height-to-gap aspect ratio),  $\Gamma$ , is set to  $\lambda/(r_o - r_i) = 1.6$ , respectively. A homogeneous magnetic field  $\mathbf{H} = H_x \mathbf{e}_x + H_z \mathbf{e}_z$  with an in axial component  $H_z$  and transversal component  $H_x$  is considered. [With  $H_z$  and  $H_x$  being the field strengths.] The length and time scales of the system are set by the gap

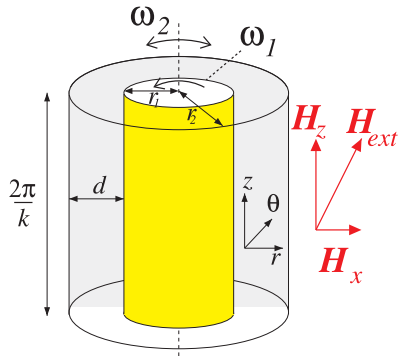


Fig. 1. Schematic of the Taylor-Couette system. Schematic of the Taylor-Couette system (TCS) with an external applied homogeneous magnetic field  $\mathbf{H}_{ext} = H_x \mathbf{e}_x + H_z \mathbf{e}_z$ . Note, that the domain is periodic in  $z$ .

width  $d = R_o - R_i$  and the diffusion time  $d^2/\nu$ , respectively. The pressure in the fluid is normalized by  $\rho\nu^2/d^2$ , and the magnetic field  $\mathbf{H}$  and the magnetization  $\mathbf{M}$  can be conveniently normalized by the quantity  $\sqrt{\rho/\mu_0}\nu/d$ , where  $\mu_0$  is the permeability of free space. These considerations lead to the following set of non-dimensionalized hydrodynamical equations [11,5]:

$$(\partial_t + \mathbf{u} \cdot \nabla) \mathbf{u} - \nabla^2 \mathbf{u} + \nabla p = (\mathbf{M} \cdot \nabla) \mathbf{H} + \frac{1}{2} \nabla \times (\mathbf{M} \times \mathbf{H}), \quad (1)$$

$$\nabla \cdot \mathbf{u} = 0.$$

On the cylindrical surfaces, the velocity fields are given by  $\mathbf{u}(r_i, \theta, z) = (0, R\omega_i, 0)$  and  $\mathbf{u}(r_o, \theta, z) = (0, R\omega_o, 0)$ , where the inner and outer Reynolds numbers are  $Re_i = \omega_i r_i d/\nu$  and  $Re_o = \omega_o r_o d/\nu$ , respectively, where  $r_i = R_i/(R_o - R_i)$  and  $r_o = R_o/(R_o - R_i)$  are the non-dimensionalized inner and outer cylinder radii, respectively.

### 2.1. Ferrohydrodynamical equation

Eq. (1) is to be solved together with an equation that describes the magnetization of the ferrofluid. Using the equilibrium magnetization of an unperturbed state in which the homogeneously magnetized ferrofluid is at rest and the mean magnetic moment is orientated in the direction of the magnetic field, we have  $\mathbf{M}^{eq} = \chi \mathbf{H}$ . The magnetic susceptibility  $\chi$  of the ferrofluid can be approximated by the Langevin's formula [13], where we set the initial value of  $\chi$  to be 0.9 and use a linear magnetization law. The ferrofluid studied corresponds to APG933 [14]. We consider the near equilibrium approximations of Niklas [15,16] with a small value of  $\|\mathbf{M} - \mathbf{M}^{eq}\|$  and small magnetic relaxation time  $\tau: |\nabla \times \mathbf{u}| \tau \ll 1$ . Using these approximations, one can obtain [11] the following magnetization equation:

$$\mathbf{M} - \mathbf{M}^{eq} = c_N^2 \left( \frac{1}{2} \nabla \times \mathbf{u} \times \mathbf{H} + \lambda_2 \mathbb{S} \mathbf{H} \right), \quad (2)$$

where

$$c_N^2 = \tau / (1/\chi + \tau \mu_0 H^2 / 6\mu \Phi) \quad (3)$$

is the Niklas coefficient [15],  $\mu$  is the dynamic viscosity,  $\Phi$  is the volume fraction of the magnetic material,  $\mathbb{S}$  is the symmetric component of the velocity gradient tensor [5,11], and  $\lambda_2$  is the *material-dependent transport coefficient* [17,5,10,32]. Using Eq. (2), we eliminate the magnetization from Eq. (1) to arrive at the following *ferrohydrodynamical equations* [5,11]:

$$\begin{aligned} (\partial_t + \mathbf{u} \cdot \nabla) \mathbf{u} - \nabla^2 \mathbf{u} + \nabla p_M \\ = -\frac{s_N^2}{2} [\mathbf{H} \nabla \cdot (\mathbf{F} + \lambda_2 \mathbb{S} \mathbf{H}) + \mathbf{H} \times \nabla \times (\mathbf{F} + \lambda_2 \mathbb{S} \mathbf{H})], \end{aligned} \quad (4)$$

where  $\mathbf{F} = (\nabla \times \mathbf{u}/2) \times \mathbf{H}$ ,  $p_M$  is the dynamic pressure incorporating all magnetic terms that can be expressed as gradients, and  $s_N$  is the *Niklas parameter* [Eq. (7)]. To the leading order, the internal magnetic field in the ferrofluid can be approximated by the externally imposed field [18], which is reasonable for obtaining the dynamical solutions of the magnetically driven fluid motion. Eq. (4) can then be simplified as

$$\begin{aligned} (\partial_t + \mathbf{u} \cdot \nabla) \mathbf{u} - \nabla^2 \mathbf{u} + \nabla p_M = s_N^2 \{ \nabla^2 \mathbf{u} - \lambda_2 [\nabla \cdot (\mathbb{S} \mathbf{H})] \\ - \mathbf{H} \times \left[ \frac{1}{2} \nabla \times (\nabla \times \mathbf{u} \times \mathbf{H}) \right] - \mathbf{H} \times (\nabla^2 \mathbf{u}) \\ + \lambda_2 \nabla \times (\mathbb{S} \mathbf{H}) \}. \end{aligned} \quad (5)$$

This way, the effect of the magnetic field and the magnetic properties of the ferrofluid on the velocity field can be characterized by a single parameter, the magnetic field or the Niklas parameter [15]:

$$s_N^2 = s_x^2 + s_z^2, \quad (6)$$

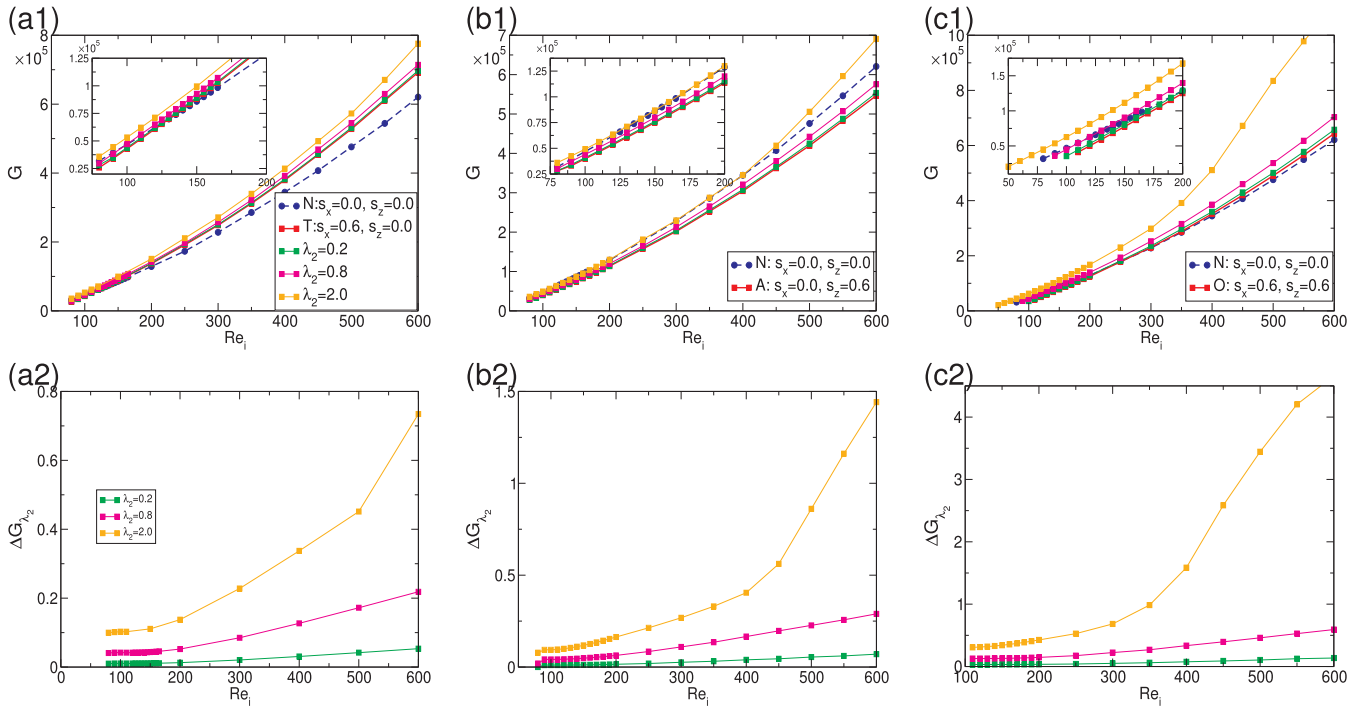


**Fig. 2.** Variation in dimensionless torque. Variation with  $Re_i$  in dimensionless torque  $G = \nu J^\omega$  for (a) transversal (T), (b) axial (A) and (c) oblique (O) magnetic field. *Top panels:* absolute torque values  $G$ ; *Bottom panels:* relative differences  $\Delta G_{\lambda_2} = G_{\lambda_2} - G_{\lambda_2=0}$ . Further parameters:  $Re_o = 0$ . The insets (in top panels) show a close up near the onset of (w) TVF.

with

$$s_x^2 = \frac{2(2 + \chi)H_x c_N}{(2 + \chi)^2 - \chi^2 \eta^2}, \quad s_z^2 = H_z c_N. \quad (7)$$

In this paper we present results in absence (none) of any applied magnetic field,  $(s_x, s_z) = (0.0, 0.0)$ , denoted **N**, and three different field configurations. A pure transverse magnetic field,  $(s_x, s_z) = (0.6, 0.0)$ , denoted **T**, for a pure axial magnetic field,  $(s_x, s_z) = (0.0, 0.6)$ , denoted **A**, and an oblique magnetic field,  $(s_x, s_z) = (0.6, 0.6)$ , denoted **O**. These values/parameters correspond to moderate magnetic fields used in several experiments [19,3].

## 2.2. Numerical methods

The ferrohydrodynamical equations of motion Eq. (4) can be solved [17,18,11] by combining a standard, second-order finite-difference scheme in  $(r, z)$  with a Fourier spectral decomposition in  $\theta$  and (explicit) time splitting. The variables can be expressed as

$$f(r, \theta, z, t) = \sum_{m=-m_{\max}}^{m_{\max}} f_m(r, z, t) e^{im\theta}, \quad (8)$$

where  $f$  denotes one of the variables  $\{u, v, w, p\}$ . For the parameter regimes considered, the choice  $m_{\max} = 16$  provides adequate accuracy. We use a uniform grid with spacing  $\delta r = \delta z = 0.02$  and time steps  $\delta t < 1/3800$ . For diagnostic purposes, we also evaluate the complex mode amplitudes  $f_{m,n}(r, t)$  obtained from a Fourier decomposition in the axial direction:

$$f_m(r, z, t) = \sum_n f_{m,n}(r, t) e^{inkz}, \quad (9)$$

where  $k = 2\pi d/\lambda$  is the axial wavenumber.

Note that for a ferrofluids in presence of a *transverse* magnetic field ( $s_x \neq 0$ ), the symmetries present in classical TCS (arbitrary rotations about the axis and the reflections about axial mid-height) are broken

and the flow is *inherently three-dimensional* for any combination of non-zero values of the parameters  $Re_i$ ,  $Re_o$  and  $s_x$  [17,3,18,11,32].

## 3. Results

It has been shown either numerical [20,21,17,11,32] and experimental [22,3,10] that *any* magnetic field stabilizes the basic state. It shift the primary (supercritical) bifurcation solutions to larger values of control parameters, with the magnitude of the shift significant to depend on the latter. Moreover, regarding elongational flow effects – expressed by the transport coefficient  $\lambda_2$ , our earlier studies [12,11] have shown, that depending on the system parameter, the effect can be either stabilizing or destabilizing (by increase of  $\lambda_2$ ) but does *not* change the general stabilizing effect of a magnetic field. Note that the present study do not focus on such ‘shift’ effects on primary onsets; however they will be mentioned if observed but not further studied in detail. To avoid such effects we consider relative values when convenient.

In the following we will focus on two main system configurations: (1) Pure inner cylinder rotation, with outer cylinder kept at rest ( $Re_o = 0$ ); (2) Counter-rotating cylinders ( $Re_o = -100$ ).

### 3.1. Inner cylinder at rest

#### 3.1.1. Torque

Consider the outer cylinder at rest, Fig. 2 presents the influence of the transport coefficient  $\lambda_2$  with variation of  $Re_i$  onto the torque  $G$  for the three different considered field orientations, (a) transversal (T), (b) axial (A), and (c) oblique (O). In calculating the torque  $G = \nu J^\omega$  we used the fact that for a flow between infinite cylinders the transverse current of the azimuthal motion,

$J^\omega = r^3 [\langle u\omega \rangle_{A,t} - \nu \langle \partial_r \omega \rangle_{A,t}]$  (with  $\langle \dots \rangle_A \equiv \int \frac{rd\theta dz}{2\pi r l}$ ), is a conserved quantity [23]. Thus the dimensionless torque is the same at the inner and the outer cylinders. The top row in Fig. 2 presents absolute values (for comparison we included the (thick dashed blue) curve in absence of any magnetic field (N)), while bottom row illustrates the differences,  $\Delta G_{\lambda_2} = G_{\lambda_2} - G_{\lambda_2=0}$ , induced due to different values  $\lambda_2$  with respect to

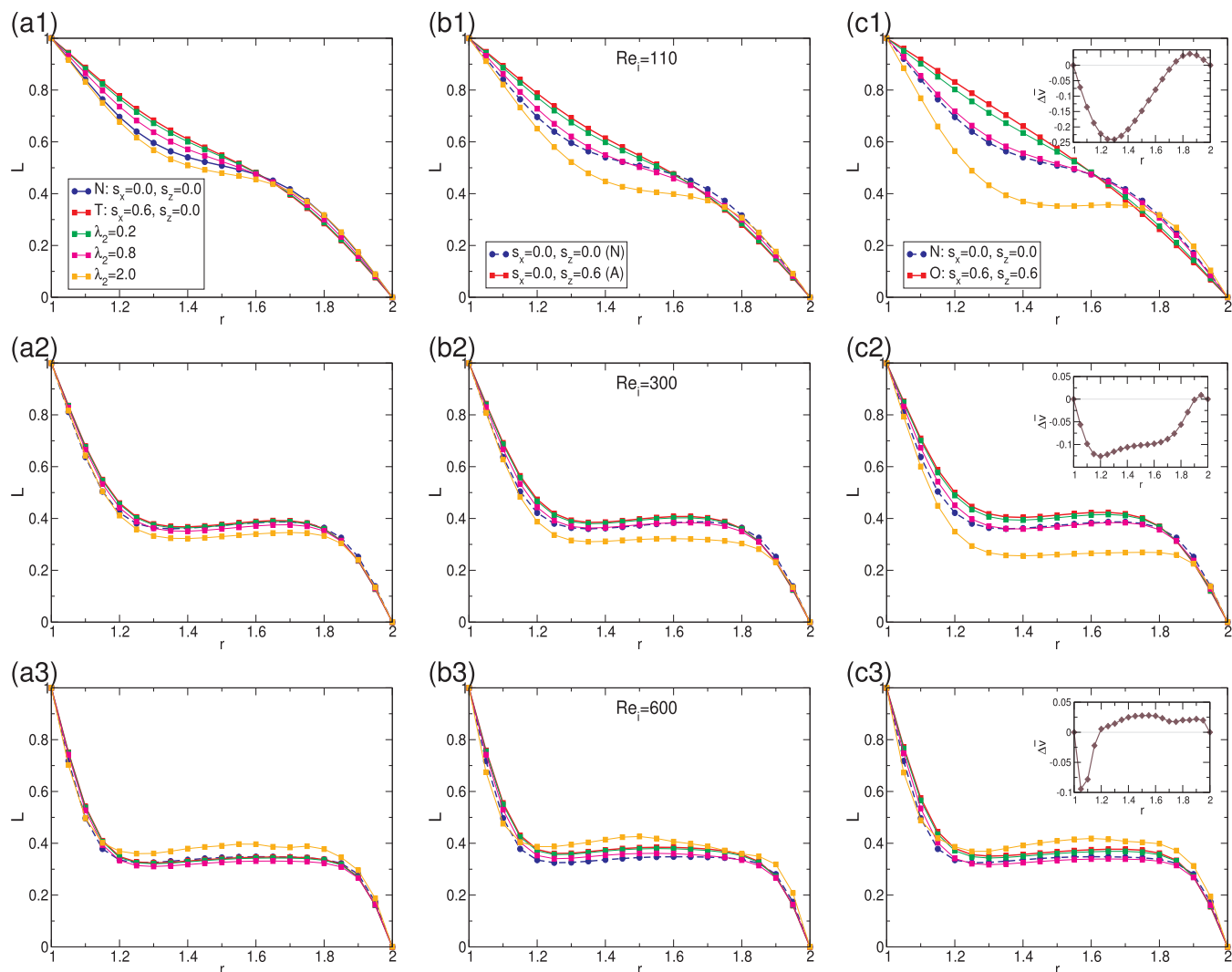


**Fig. 3.** Variation in angular momentum. Variation of angular momentum  $L(r) = r\langle v(r) \rangle_{\theta,z} / Re_i$  versus the radius  $r$  for (w) TVF at  $Re_o = 0$  for (a) transversal (T), (b) axial (A) and (c) oblique (O) magnetic field. (N) notes the situation in absence of any applied magnetic field. *Top row:*  $Re_i = 110$ ; *middle row:*  $Re_i = 300$ ; *Bottom row:*  $Re_i = 600$ . The insets in (c) illustrate the (scaled) differences in azimuthal mean velocities  $\Delta \bar{v} = (\langle v_{\lambda_2=2.0}(r) \rangle_{\theta,z} - \langle v_{\lambda_2=0.0}(r) \rangle_{\theta,z}) / Re_i$ , in oblique fields for large value  $\lambda_2 = 2.0$  and absence of it (see also Fig. 8).

the corresponding magnetic field without any considered elongational flow ( $\lambda_2 = 0$ ). The insets show a close up near the onset of (w) TVF and illustrate the shift in bifurcation thresholds, which can be either stabilizing or destabilizing, depending on the combination of magnetic field and  $\lambda_2$  [12,11]. In general the torque  $G$  increases monotonous with  $Re_i$  (Fig. 2 top panels) and curves considering finite values  $\lambda_2$  are lying above the one without any considered elongational flow ( $\lambda_2 = 0$ ). Note, the terminus elongational flow incorporates either agglomeration and chain formation. Further the differences  $\Delta G_{\lambda_2}$  (Fig. 2 bottom panels) continuously enlarge with increasing value  $\lambda_2$ . That is because at larger  $Re_i$ , higher agglomeration of particles and/or larger chains hinder the ‘free’ or ‘smooth’ motion of the fluid and thus increase its torque. Consequently this effect increases with larger values  $Re_i$  and in particular for large considered value  $\lambda_2 = 2.0$ . There is an obvious large influence, consider such strong elongational flow, as the corresponding curves (Fig. 2 bottom panels) show a significant change in slope - they become steeper. The (exact) value for change in slope depends on the field configuration and goes from  $Re_i \approx 500$  in transversal (T) over  $Re_i \approx 400$  in axial (A) to  $Re_i \approx 350$  in oblique (O). Physically the steeper curves in torque  $G$  with increasing  $\lambda_2$  results from the fact that the flow becomes more inert having larger particle chains and or aggregation inside (i.e. identified by larger  $\lambda_2$ ) which result in larger torque response

for otherwise fixed parameters.

### 3.1.2. Angular momentum transport

To attempt to characterize the agglomeration phenomenon, i.e. the influence and modifications, due to finite values  $\lambda_2$ , onto the flow structures we further examine the behavior of the angular momentum  $L(r)$ . Fig. 3 show the mean (axially and azimuthally averaged) angular momentum  $L(r) = r\langle v(r) \rangle_{\theta,z} / Re_i$ , as a function of the radius  $r$  for three different values  $Re_i = 110, 300, 600$  (see also Fig. 2).

In general, the profiles indicate typical behavior in that positive angular momentum decreases outward from the inner cylinder. While this process is relatively small for  $Re_i = 110$  (top row) it becomes more pronounced for  $Re_i = 300$  and even stronger for 600, resulting in a region of nearly constant angular momentum in the center of the annulus. This horizontal plateau in the middle of the gap is most pronounced for larger value  $Re_i = 600$ , and tends to be slightly closer the inner cylinder than the outer cylinder. In general the angular momentum curves follow a monotonically varying trend with increase in  $\lambda_2$ . For large values  $\lambda_2$  the curves show the largest modifications, in particular for oblique (Fig. 3(c)) magnetic fields (O). In detail, for small Reynolds number  $Re_i = 110$ , an increase in  $\lambda_2$  results in changing and formation of the horizontal plateau in the center. At moderate values  $Re_i$  this

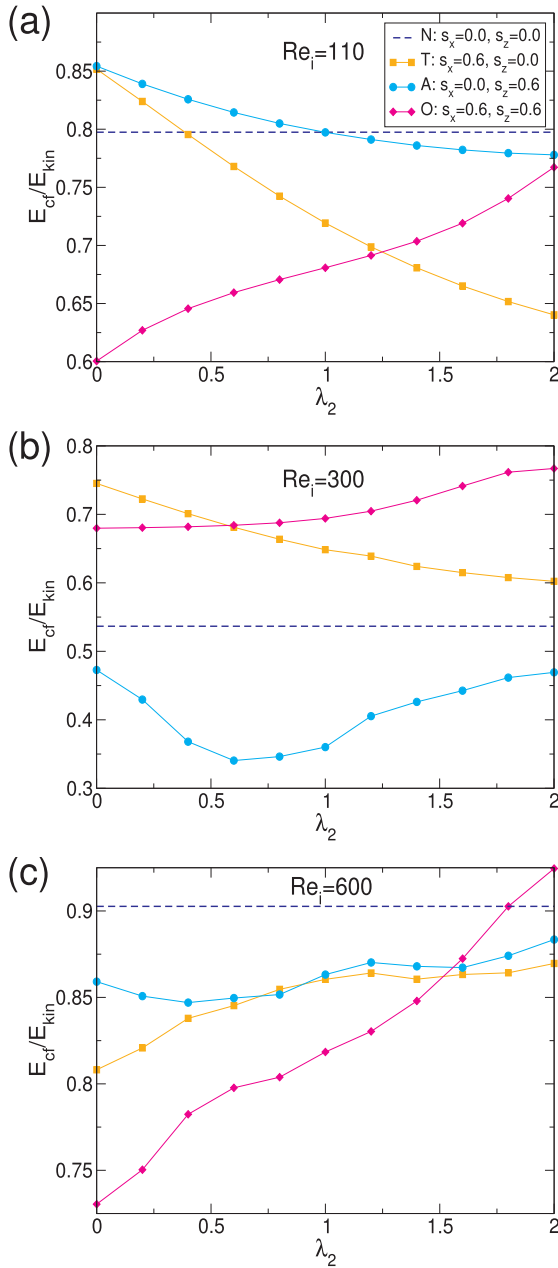


**Fig. 4.** Variation in relative energy amount/content. Variation of the relative energy amount/content (cross-flow and kinetic)  $E_{cf}/E_{kin}$  with  $\lambda_2$  in T, A and O field configuration, for  $Re_o = 0$  and (a)  $Re_i = 110$ , (b)  $Re_i = 300$  and (c)  $Re_i = 600$ , respectively.

horizontal plateau is already fully formed and increasing  $\lambda_2$  moves the level of the plateau to lower values  $L$ ; this effect is similar for all field configuration, while it is largest for oblique fields. At larger values  $Re_i$  the plateau is more pronounced (it is wider expanded in radial direction  $r$ ) in general. Also here an increase in  $\lambda_2$  changes the level. For small and moderate  $\lambda_2$  it also moves towards smaller values  $L$ , before at larger values  $\lambda_2$  it moves into opposite direction, it moves to larger values  $L$ . Moreover for large  $\lambda_2$  the plateau changes its shape as it develops a more ‘bow-like’ shape characteristics with a peak in the center region. In particular in axial field configuration this peak is well visible (bottom panel in Fig. 3(c)). Further observation for any field configuration is, that with increasing  $\lambda_2$  the curves become steeper at the inner and outer cylinder.

The insets in Fig. 3(c), illustrate the (scaled) differences in

azimuthal mean velocities  $\Delta \bar{v} = (\langle v_{\lambda_2=2.0}(r) \rangle_{\theta, z} - \langle v_{\lambda_2=0.0}(r) \rangle_{\theta, z})/Re_i$  (for oblique fields), for strong considered elongational flow, i.e. for large value  $\lambda_2 = 2.0$  and absence of it ( $\lambda_2 = 0.0$ ). In general  $\Delta \bar{v}$  is negative close to the inner and positive close to the outer cylinder, respectively. An explanation is that the agglomerated particles and/or longer chains are transported towards the (stationary) outer cylinder. Due to their size they slow down and decrease the averaged in this outer bulk region. Increasing  $Re_i$  the region with  $\Delta \bar{v} < 0$  is moving towards the inner cylinder.

Summarizing one can say, that the elongational flow effect and the here form resulting flow structural modifications becomes more pronounced the larger the inner cylinder rotation,  $Re_i$ .

### 3.1.3. Energy contents

A typical global measure to characterize the flow is the modal kinetic energy defined as

$$E_{kin} = \sum_m E_m = \frac{1}{2} \int_0^{2\pi} \int_{-\Gamma/2}^{\Gamma/2} \int_{r_i}^{r_o} \mathbf{u}_m \mathbf{u}_m^* r dr dz d\theta, \quad (10)$$

where  $\mathbf{u}_m$  ( $\mathbf{u}_m^*$ ) is the  $m$ -th (complex conjugate) Fourier mode of the velocity field,  $E_{kin}$  is constant (non-constant) for a steady (unsteady) solution. Note that for diagnostic purpose we will consider the time-averaged energy  $\bar{E}_{kin} = \int_0^T E_{kin} dt$ , averaged of a period of the respective flow solution. Another quantity, which is also used as typical indication of flow characteristics, often used for turbulent analysis, is given by the cross-flow energy [24],

$$E_{cf} = \frac{1}{2} \int_0^{2\pi} \int_{-\Gamma/2}^{\Gamma/2} \int_{r_i}^{r_o} (u_m^2 + w_m^2) r dr dz d\theta. \quad (11)$$

The cross-flow energy  $E_{cf}$  measures the instantaneous energy associated with the radial and axial velocity components.

Avoiding to have to deal with the different stability ‘shifts’ [17,12], we will consider the relative value, the relation of both energy contents,  $E_{cf}/E_{kin}$ , in order to compare the influence of the elongational flow effects. Note (as for  $E_{kin}$ ), for a diagnostic purpose, we may consider the time-averaged (over one period) quantities.

Fig. 4 shows the variation of the relative energy amount  $E_{cf}/E_{kin}$  with  $\lambda_2$ . At small  $Re_i = 110$  the ratio monotonically decreases with increasing  $\lambda_2$  for either pure transversal or axial magnetic field. Similar scenario is found for  $Re_i = 300$  and transversal field. Interestingly the behavior is just opposite, it is monotonously increasing, for an oblique magnetic field at small and moderate values  $Re_i = 110$  and  $Re_i = 300$ . However, it starts at a much smaller value. It is worth to mention that for any investigated  $Re_i$ , the absolute values  $E_{cf}$  and  $E_{kin}$  are mainly monotonously increasing with  $\lambda_2$  (only exception is the axial field at  $Re_i = 300$ ). The different shape of the curves is based on the fact, that in the different field configurations,  $E_{cf}$  and  $E_{kin}$  increase ‘fast’ with respect to  $\lambda_2$ . Pure transversal and pure axial field show qualitative the same tendency, while oblique fields behave different. For the latter, the relative value  $E_{cf}/E_{kin}$  always increases with  $\lambda_2$ , independent of the field configuration. At  $Re_i = 600$ , the ratio  $E_{cf}/E_{kin}$  increases for any field configuration, which is most pronounced for oblique field configuration.

## 3.2. Counter-rotating cylinders

After the situation with inner cylinder at rest, we come now to the situation with both cylinders in motion, in particular in counter-rotating configuration.

### 3.2.1. Torque

Fig. 5 shows the torque  $G$  and differences  $\Delta G$  with variation  $Re_i$  and counter-rotating outer cylinder  $Re_o = -100$ . Compared to the situation with outer cylinder at rest (Fig. 2), the curves show more variation. In particular the behavior of  $\Delta G$  is different. The insets illustrate again a

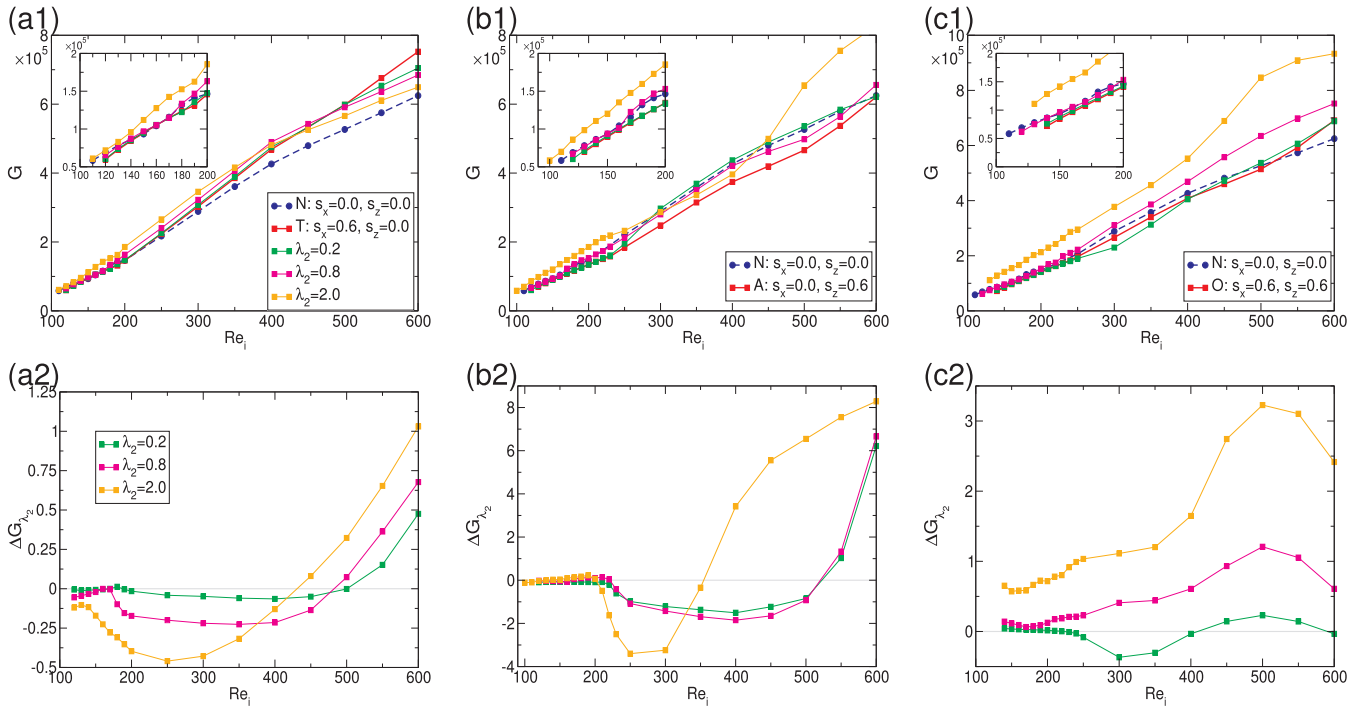


Fig. 5. Variation in dimensionless torque. As Fig. 2 but for counter-rotating cylinders with  $Re_o = -100$ . Note the different scaling on the ordinate  $\Delta G_{\lambda_2}$ .

shift in the onsets of primary bifurcations with respect to different values  $\lambda_2$ . However more interesting is the fact, that the curves for different values  $\lambda_2$  intersect. They are *not* continuously increasing with  $\lambda_2$  anymore. As a result the differences  $\Delta G$  is *not* monotonous and has either positive and negative values. For axial (A) and transversal (T) field configuration (Fig. 5(a, b)) the behavior is very similar. Here an initial increase of  $\Delta G$  with  $Re_i$  (either absolute in positive or negative region) is followed by a decrease in  $\Delta G$  to (stronger) negative values at smaller  $Re_i$ . This behavior is stronger and more pronounced for larger values  $\lambda_2$ . Here after at larger  $Re_i$  there is a significant increase in  $\Delta G$ , in particular for  $\lambda_2 = 2.0$ . Consider the oblique field configuration (Fig. 5(c)), the behavior remains the same for small values  $\lambda_2$ . However, at larger values  $\lambda_2$  there is no decrease and no negative values in  $\Delta G$  are observable at moderate  $Re_i$ , anymore. Interestingly for any considered  $\lambda_2$ , the differences  $\Delta G$  decreases at large  $Re_i$ .

This finding of an initial maximum peak in  $\Delta G$  with increasing  $Re_i$  is similar to the observations by Storozhenko et al. [9]. They studied different diluted ferrofluid concentrations under the influence of an oscillatory magnetic field. Large concentration of aggregates in the ferrofluids resulted in a local maximum (peak) in the torque with respect to the oscillatory field frequency. Also we do not have an oscillatory field, but increasing  $Re_i$  changes the contribution of aggregates to the rotational effect in a similar way. Thus for small  $\lambda_2$  the effect is very weak, the local maximum is small, which significant increases for larger values  $\lambda_2$ . Due to counter-rotating cylinders the shear in the bulk increases and the effect of agglomeration becomes more important. Thus the torque initially increases with  $Re_i$  until a critical value, at which a (typical minor) rearrangement of the flow within the bulk happen, and hereafter increases slower. This rearrangement are either move of vortex center are in extreme cases (only seen for oblique field the elimination of one toroidally vortex pair).

### 3.2.2. Angular momentum transport

As we now consider counter-rotating cylinders, the profiles indicate typical behavior in that positive angular momentum decreases outward from the inner cylinder and opposite, negative angular momentum decreases inward from the outer cylinder. This process becomes

stronger with increasing  $Re_i$ , resulting in a flat region of nearly constant and close to zero angular momentum in between.

Fig. 6 illustrates the angular momentum in counter-rotating situation at different  $Re_i$ . Overall it shows more variation, in particular for oblique field, than seen before in absence of outer cylinder rotation (Fig. 3). In general one can say, larger values  $\lambda_2$ , result in stronger modification of the profiles. For small  $Re_i$  the S-shape of the curves increases together with  $\lambda_2$ , while for moderate  $Re_i$  the central plateau region is mainly shifted towards lower values  $L$  with increasing  $\lambda_2$ . At large  $Re_i$  the changes are more versatile and *not* unidirectional. However, all over for  $\lambda_2 = 2.0$  one sees the largest/strongest modifications, and even the development of local extrema - a local minima to be concrete, within the plateau region (cf. Fig. 6(b) at  $Re_i = 300$  and (c) at  $Re_i = 600$ ). In particular this local minimum, also moves towards the inner cylinder with larger value  $\lambda_2$ . As a result the main central plateau region becomes smaller. This effect is also visible in the insets showing the differences in azimuthal mean velocities  $\Delta \bar{v}$ . As for outer cylinder at rest,  $\Delta \bar{v}$  is negative close to the inner cylinder. While for small and large  $Re_i$ ,  $\Delta \bar{v}$  also shows the same behavior as for outer cylinder at rest, the shape is different, mainly at medium  $Re_i$ , here  $\Delta \bar{v}$  is also negative near the outer cylinder.

One explanation is that the agglomerated particles and/or longer chains are transported towards the (stationary) outer cylinder. Due to their size they slow down and decrease the averaged velocity in this outer bulk region. Increasing  $Re_i$  the region with  $\Delta \bar{v} < 0$  is moving towards the inner cylinder.

The variation of the relative energy amount  $E_{cf}/E_{kin}$  with  $\lambda_2$  for considered counter-rotating cylinders is presented in Fig. 7. Here also all absolute values are monotonously increasing with  $\lambda_2$ . At low  $Re_i$  one can see the same characteristics as for outer cylinder at rest. For transversal and axial field configuration the values  $E_{cf}/E_{kin}$  mainly decrease while for oblique field they increase. However this change at moderate  $Re_i = 300$ , for which all curves increase with  $\lambda_2$  independent of the field configuration. As before in general the values  $E_{cf}$  and  $E_{kin}$  are monotonously increasing with  $\lambda_2$ . It is only the rate/relation between both, which one increases faster, that result in moving up or down with  $\lambda_2$ . The reason for the different behavior of  $E_{cf}/E_{kin}$  for

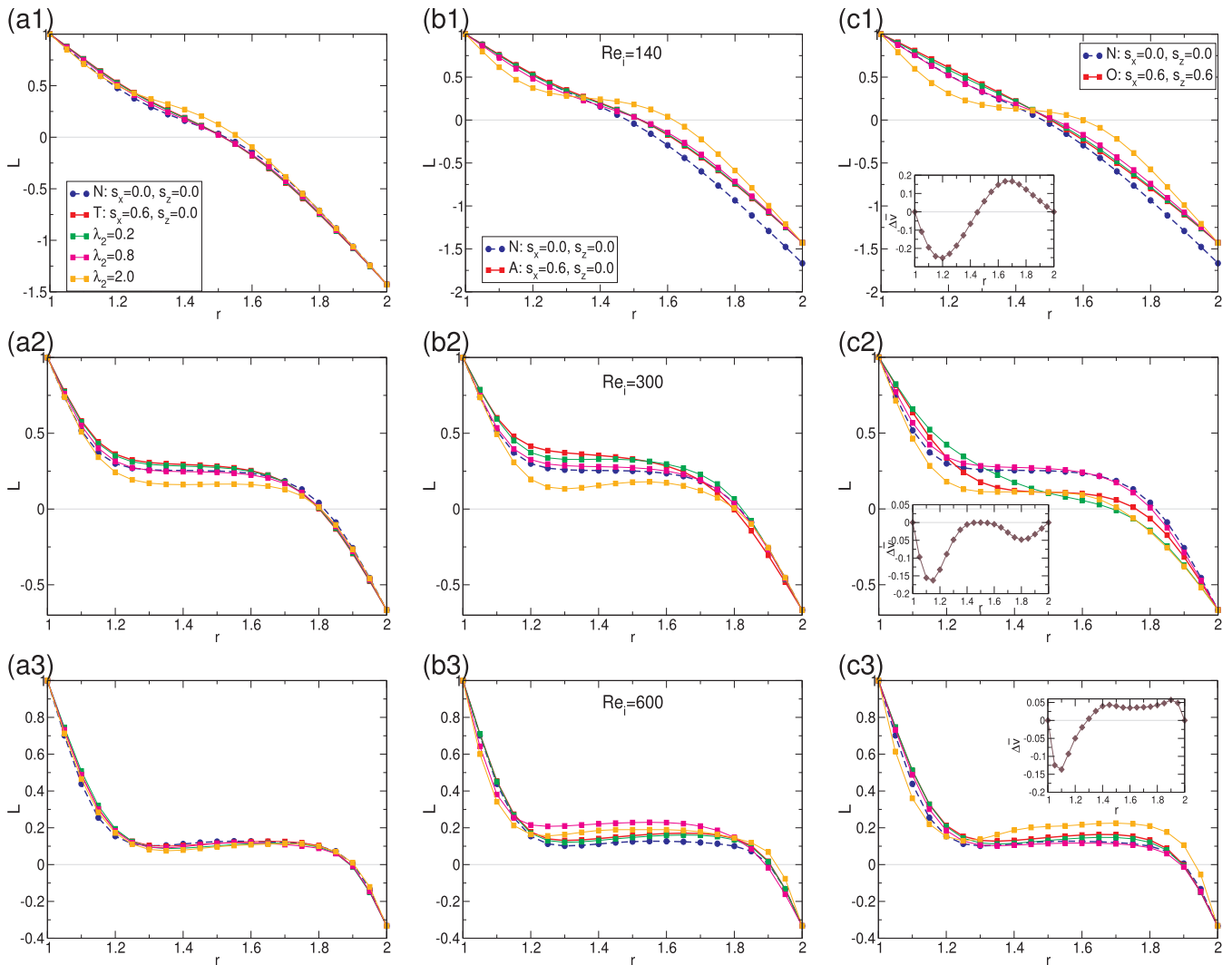


Fig. 6. Variation in angular momentum. As Fig. 3 but for counter-rotating cylinders with  $Re_o = -100$  and (a)  $Re_i = 140$ , (b)  $Re_i = 300$  and (c)  $Re_i = 600$ , respectively.

oblique field can be understood in the mode interaction for such a field with the additional stimulation of  $m = \pm 1$  modes [17,32]. These modes appear in the term with the transport coefficient  $\lambda_2$  entering the ferrohydrodynamic Eq. (5). However their relative contribution becomes smaller with increasing Reynolds numbers  $Re_{i,o}$ . Physically speaking this means the stronger the driving forces of the flow are, the less relevant are microscopic variations (at least as long they are relatively small).

For counter-rotating cylinders another possible quantity to study the influence of elongation/agglomeration, the influence of transport coefficient  $\lambda_2$ , is the azimuthal and axial averaged velocity  $\langle v(r) \rangle_{\theta,z}$ . In particular we will focus on its zero crossing with respect to the radial position in order to see the modifications due to  $\lambda_2$ .

Fig. 8 shows the variation with  $\lambda_2$  of the radial position at which the axial and azimuthal averaged velocity  $\langle v(r) \rangle_{\theta,z} = 0$  vanishes. First of all it is obvious that in general with increasing  $Re_i$ , as expected, the zero-crossing moves outward towards the outer cylinder (compare ordinates in Fig. 8). Starting with small value  $Re_i = 140$  (Fig. 8(a)), one sees that for pure transversal and axial fields the radial position remains almost unchanged until a value of  $\lambda_2$  at about 1.4. For larger values  $\lambda_2$  the zero crossing moves in opposite directions, outwards for axial and inwards for transversal field. In both cases the behavior is monotonous with increase in  $\lambda_2$ . However, for oblique magnetic field the latter does not hold anymore, the variation is way more complex/versatile. Here the position changes first outwards before it changes inwards with

increasing  $\lambda_2$ . At larger value  $Re_i = 300$  (Fig. 8(b)) the change under axial and transversal field are in the same direction; the zero-crossing point moves monotonously towards the inner cylinder, whereby the radial coordinate is always smaller for transversal field. Although for oblique field one sees again a complex, non-monotonous change with variation in  $\lambda_2$ , the general tendency follows the both other field configurations (at least for values  $\lambda_2$  larger than 0.8); it is mainly inward directed. A slightly outward move at small  $\lambda_2$  is followed by an inward move of the radial coordinate of the zero crossing line; in particular at large  $\lambda_2$  the inward move becomes significant.

Finally, at larger  $Re_i = 600$  (Fig. 8(c)) the radial position only changes minor with respect to  $\lambda_2$ , independent of the field configuration. While for transversal and axial magnetic field the curve shows a wave-like motion with small variations, for oblique field an almost monotonous move outward is observed.

### 3.3. Dominant modes

Depending on the different system parameters, in particular  $Re_i$ ,  $Re_o$ ,  $s_x$  and  $s_z$  the detected flow structures have different dominant modes. However, for all here investigated flow states the axisymmetric mode  $m = 0$  is always predominant! On top of these we find the dominant modes to be either  $m = 2$  (field induced for  $s_x \neq 0$ ),  $m = 1$  and/or combination of both. Which one are exactly present depend on all former mentioned parameters. Table 1 gives an overview of the

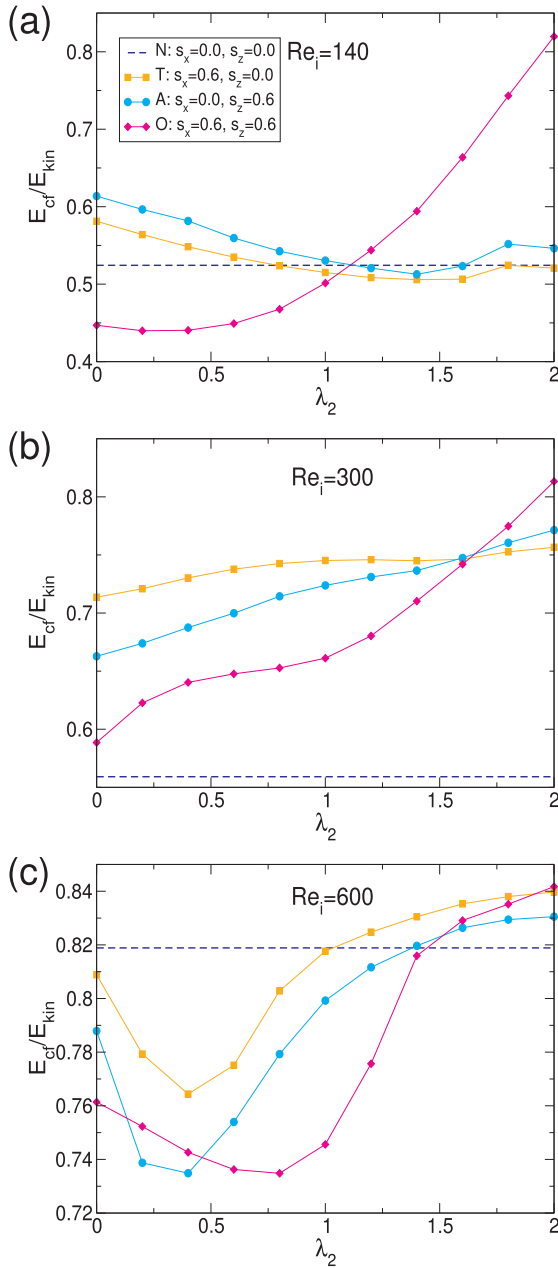


**Fig. 7.** Variation in relative energy amount. As Fig. 4 but for  $Re_o = -100$  and (a)  $Re_i = 140$ , (b)  $Re_i = 300$  and (c)  $Re_i = 600$ , respectively. Note the different scaling on the ordinate  $E_o/E_{kin}$ .

dominant modes regarding the considered parameters.

The radial position of vortex center in the bulk (Fig. 9), depends on the strength of considered elongational flow, i.e. transport coefficient  $\lambda_2$  (see also Figs. 10 and 11). For T field configuration the result is an outward move of the centers with increasing value  $\lambda_2$ , either for outer cylinder at rest or counter-rotating cylinders. The same applies initially for O field configuration for values  $\lambda_2 \lesssim 1.1$  before for larger values  $\lambda_2$  the effect is reversed.

Physically an increasing value  $\lambda_2$ , means larger effect of agglomeration, aggregation and larger chain lengths (just opposite of having more diluted ferrofluid): thus the movement of the flow becomes more inert due to larger required moments. As other parameters are fixed (e.g.  $Re_{i,o}$ ) the vortex center move outwards for compensation. This effect is quantitative much stronger for oblique field. Note that for flows in O field the situation is general complexer, as the vortex centers of the

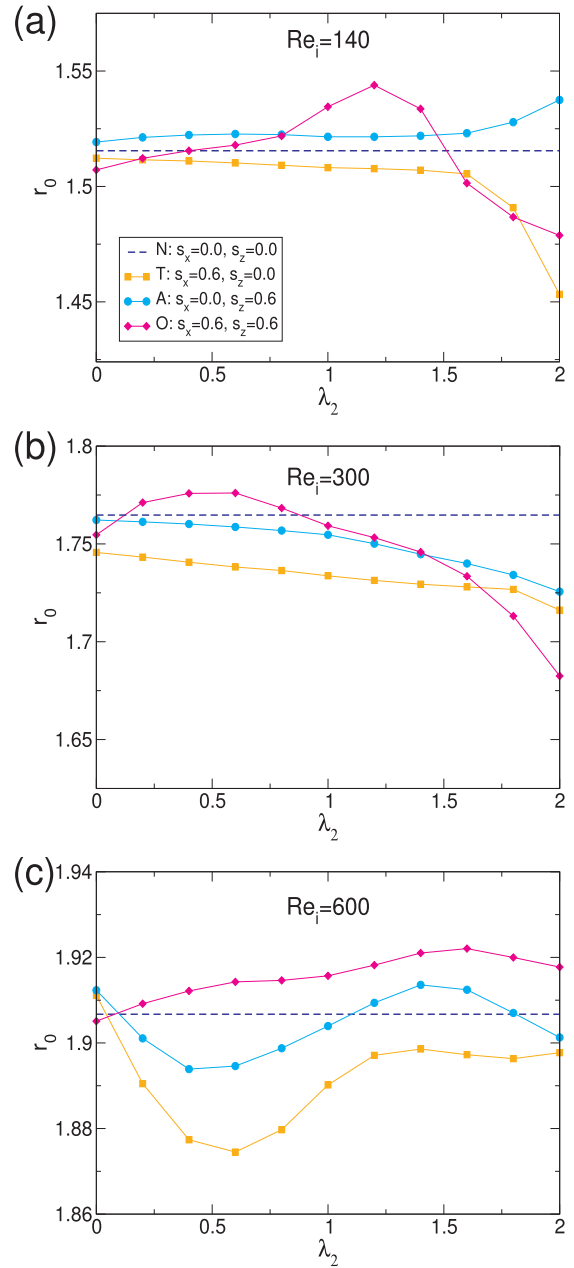


**Fig. 8.** Variation of the radial position of azimuthal zero flow. Variation with  $\lambda_2$  of the radial position of  $r_0 = r(\langle v(r) \rangle_{\theta,z} = 0)$  for  $Re_o = -100$  and (a)  $Re_i = 140$ , (b)  $Re_i = 300$  and (c)  $Re_i = 600$ , respectively. Note that the scale for radial position is non-dimensionalized with inner cylinder at  $r_i = 1$  and outer one at  $r_o = 2$ , respectively. The dashed line represents the corresponding zero-crossing position in absence of any magnetic field.

counter-rotating vortex pair becomes more and more out of their alignment (speaking in  $r$ ) and become intertwined (see two curves in Fig. 9 for O field configuration). This makes an accurate determination of the center position rather difficult. However, the different behavior for oblique field with the vortex center moving inwards again for larger  $\lambda_2$  can be understood due to the different dominant mode amplitude  $m = 1$ , which is a direct result of the non-linear interaction of axial and transverse field (stimulating additional non-symmetric  $m = \pm 1$  modes [17,32]). These additional stimulated helical modes result in strengthening the azimuthal ( $\theta$ ) flow components, in particular in the outer region. Thus having larger transport coefficient  $\lambda_2$  means stronger agglomeration, aggregation and larger ferrofluid chains. Thus regions can be seen as slug flow and thus 'push' the vortex center inwards again.

**Table 1**  
Investigated parameter sets. Parameter sets,  $Re_i$ ,  $Re_o$ , field configuration  $\{T, A, O\}$  and dominant modes  $m$  within the appearing flow structures at  $0 \leq \lambda_2 \leq 2.0$ .

$Re_i$	$Re_o$	field	$m$
110	0	T	2
		A	0
		O	1
300	0	T	2
		A	0, 1
		O	1
600	0	T	1
		A	1
		O	1
140	-100	T	2
		A	0
		O	1
300	-100	T	2
		A	2
		O	1
600	-100	T	1
		A	1
		O	1

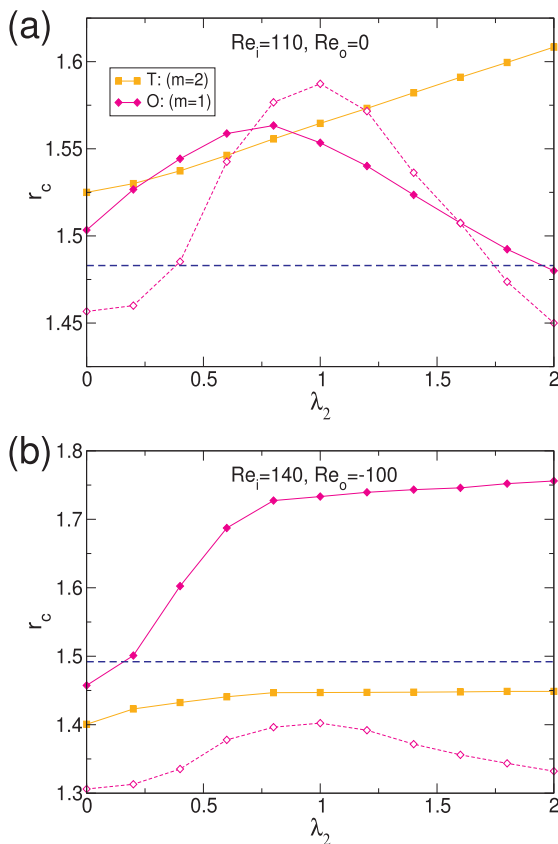


**Fig. 9.** Variation of the radial position of vortex center. Variation with  $\lambda_2$  of the radial position of  $r_c$  for (a)  $Re_i = 110$ ,  $Re_o = 0$  and (b)  $Re_i = 140$ ,  $Re_o = -100$ , respectively. Note that the scale for radial position is non-dimensionalized with inner cylinder at  $r_i = 1$  and outer one at  $r_o = 2$ , respectively. The horizontal dashed line represents the corresponding zero-crossing position in absence of any magnetic field.

Such behavior is also confirm with the observation of strong negative azimuthal mean velocities  $\Delta \bar{v}$  as presented in the insets in Figs. 3 and 6. This behavior applies similar for outer cylinder at rest and counter-rotating cylinders. Moreover in the case of counter-rotating cylinders either for transverse and oblique field (Fig. 9(b)) one sees a stagnation

at a specific radial position.

### 3.4. Flow structures

#### 3.4.1. Transversal and oblique field

Fig. 10 elucidates selected flow structures for outer cylinder at rest  $Re_o = 0$  in either transversal (a,c) and oblique (b,d) field configuration with and without considered transport coefficient  $\lambda_2$  as indicated at  $Re_i = 110$  and  $Re_i = 300$ . Although the flow structures in transversal field T at  $Re_i = 110$  and  $Re_i = 300$  (Fig. 10(a, c)) are both  $m = 2$  wavy vortices (2-wTVF), they are crucially different. The one at lower  $Re_i = 110$  is a *non-rotating*, transversal field induced wavy vortex flow state [17]. In absence of the symmetry breaking transversal field only pure TVF exists. The onset for classical (azimuthal rotating) 2-wTVF is at  $Re_i$  about 118. In contrast these 2-wTVF at  $Re_i = 300$  also exist aside/without of any applied magnetic field, only becomes further modified due to presence of such magnetic field. In particular the classical 2-wTVF is an azimuthal rotating flow state. For the complexer oblique field configuration (Fig. 10(b, d)) on the other hand we observed 1-wTVF, for which the  $m = 2$  mode influence due to the symmetry breaking transversal field is clearly visible in all flow structures (see in particular plots of azimuthal vorticity  $\eta(r, \theta = 0, z)$  and the radial velocity  $u(r = 0.5, \theta, z)$  on an unrolled cylindrical surface in the annulus at mid-gap). Contrary for T field configuration, under O field all 1-wTVF structures are rotating. Note the onset of 1-wTVF in absence of any field is at  $Re_i$  about 108. Regarding T field configuration (Fig. 10(a, c)) the vector plot  $[u(r, z), w(r, z)]$  of the radial and axial velocity components illustrate the former presented radial ‘outward’ shift of the center position of the vortices (see Fig. 9). Moreover, with increasing  $\lambda_2$  we found for rotating wavy vortex flow (1-wTVF and 2-wTVF) the both centers of the counter-rotating vortex pair to become more separated in it’s radial position; as a result the flow structures become more intertwined.

Consider counter-rotating cylinders  $Re_o = -100$  (Fig. 11) the flow structures become more pronounced in general, but keep the same main characteristics as discussed for outer cylinder at rest (Fig. 10). Flow structures in T field configuration (Fig. 11(a, c)) remain mode-2 dominated (2-wTVF) and those in O field configuration (Fig. 11(b, d)) remain mainly (see below) mode-1 dominated (1-wTVF). The additional rotation of the outer cylinder results in more intertwined flow dynamics within the bulk. While for T field and  $Re_i = 140$  the 2-wTVF are *non-rotating* structures, they do *rotate* for  $Re_i = 300$ . Interestingly the 2-wTVF for O at  $Re_i = 140$  and strong considered elongational flow  $\lambda_2 = 2.0$  changes to be mode-2 dominant. Moreover it is not a 2-wTVF anymore, it shows various features and characteristics typical for mode-2 Mixed-Cross-Spiral solution (MCS) [25], as interaction of helical spiral flow states. In fact the amplitudes of modes  $m = 2$  and  $m = -2$  are almost identical, it is even close to a 2-Mixed-Ribbon solution.

Regarding Figs. 10 and 11 it is quite obvious that the flow structures become more complex/difficult with increasing  $\lambda_2$ . This is best visible in either the 3D isosurface plots of  $r_v$ , which become more scattered and complexer on the its surface. Here it is worth to mention, that the azimuthal vorticity of the flow structures also increases (here not shown) almost linear with  $\lambda_2$ , which we deeply studied in a previous work [11]. Similar the radial velocity  $u(r = 0.5, \theta, z)$  on an unrolled cylindrical surface in the annulus show significant stronger variation in its contours and velocity strength.

#### 3.4.2. Axial field

A pure axial field only shift the onsets of instabilities, it’s bifurcation thresholds to larger values (it stabilizes the basic state) and does *not* modify the flow structures [17,22]. This also hold for further considered elongational flow! Thus, the study of only this field configuration is somehow relative boring. However, we do not want miss to present at least one flow structure in pure axial magnetic field configuration. In particular we did an interesting observation. Fig. 12

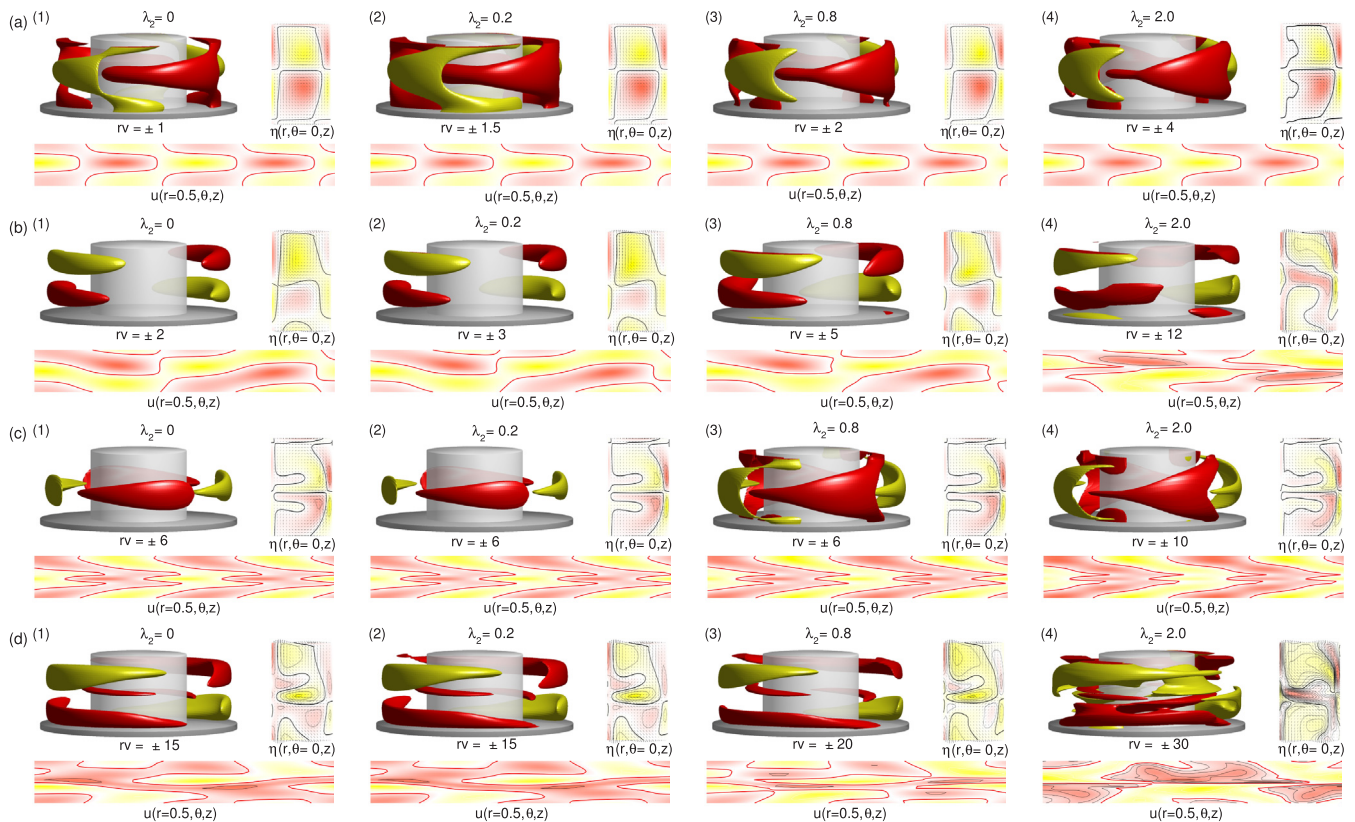


**Fig. 10.** Flow visualizations for  $Re_0 = 0$ . Variation of flow structures with  $\lambda_2$  in (a, c) transversal field and (b, d) axial field, respectively. Control parameters are (a, b)  $Re_i = 110$ , (c, d)  $Re_i = 300$  and (1)  $\lambda_2 = 0.0$ , (2)  $\lambda_2 = 0.2$ , (3)  $\lambda_2 = 0.8$  and (4)  $\lambda_2 = 2.0$ . Each sub-panel shows (starting top left and going clockwise) isosurfaces of  $rv$  [red (dark gray) and yellow (light gray) colors correspond to positive and negative values, respectively, with zero specified as white], vector plot  $[u(r, z), w(r, z)]$  of the radial and axial velocity components (including the azimuthal vorticity  $\eta(r, \theta = 0, z)$ ) and the radial velocity  $u(r = 0.5, \theta, z)$  on an unrolled cylindrical surface in the annulus at mid-gap [red (yellow) color indicates in (out) flow]. (For interpretation of the references to colour in this figure legend, the reader is referred to the web version of this article.)

illustrate the flow structure in an axial magnetic field  $A$  at  $Re_i = 600$  and  $Re_o = 0$  with  $\lambda_2 = 0.2$ . Obvious this is an  $m = 1$  mode flow, a ‘classical’ 1-wTVF with azimuthal rotation, which is the most common/representative one for all detected flows under axial field geometry (see also Table 1). Interestingly the shown 1-wTVF (Fig. 12) has aside its dominant  $m = 1$  mode a quite strong contribution of the  $m = -1$  mode as visible in either isosurface plot  $rv$  and radial velocity  $u(r = 0.5, \theta, z)$  on an unrolled cylindrical surface. This is similar to the previous mentioned finding of and Mixed-Cross-Spiral-like structure (Fig. 11(b4)). However, here with interaction of  $m = 1$  and  $m = -1$  helical modes, which means it is an (close to) 1-MCS solution [25]. To our knowledge such a flow has not been reported yet without artificial symmetry restrictions.

#### 4. Discussion and conclusion

While the flow in non structured ferrofluids can be described by the influence of the field on the relaxation of the magnetization of the fluid [7,22] flow effects in fluids with interaction (as here considered elongational flow, which describes the effect of agglomeration, aggregation and chain formation) will require a more complex theoretical description.

As a foundational paradigm of fluid dynamics, the Taylor-Couette system (TCS) has been extensively investigated computationally and experimentally. In spite of the long history of the TCS and the vast literature on the subject, the dynamics of TCS with a complex fluid subject have begun to be investigated relatively recently. In fact, although the nonlinear dynamics in counter-rotating TCS has been extensively studied the knowledge of the non-linear dynamics in this

regime for complex fluids, in particular ferrofluids is very rare. The present work is aimed to fill this gap.

In particular, we explored the effect of elongational flow on ferrofluid in the presence of transverse, axial and oblique magnetic field, we consider the so-called *transport coefficient*  $\lambda_2$  on the TCS with either outer cylinder at rest or cylinders in counter-rotating scenario. Note that in this study we do not focus on the well-known stabilization effect for any magnetic field, as the onset of centrifugal instability is relatively shifted in the bifurcation curve [3,18,17,26].

In general one can say that in many ways elongational flow enhances the effect of magnetic fields, independent of its configuration (transversal (T), axial (A) and oblique (O)).

Investigating the dimensionless torque  $G$  we observed modification due to  $\lambda_2$ , which are stronger for larger values  $\lambda_2$ . While for outer cylinder at rest  $Re_o = 0$  these modifications grow monotonically with increasing  $Re_i$ , the counter-rotating situation is more complex. Regarding the difference  $\Delta G$  with respect to neglected elongational flow ( $\lambda_2 = 0$ ), an initial small increase is followed by a decrease, before a significant increase, with enlarging  $Re_i$ . This holds for all considered field geometries (A,T,O) and is the largest for larger  $\lambda_2$ . This largest effect can be understood as with increasing  $\lambda_2$  the flow becomes more inert having larger particle chains and or aggregation inside (i.e. identified by larger  $\lambda_2$ ) otherwise fixed parameters.

Such observations confirm the studies by Storozhenko et al. [9] who investigated different concentrations of ferromagnetic particles under a rotating magnetic field. They detected a field driven agglomeration of particles in case of stationary field at different orientation, which becomes destroyed for faster rotations. In their case the destruction of agglomeration can be seen in a decreasing torque with increasing

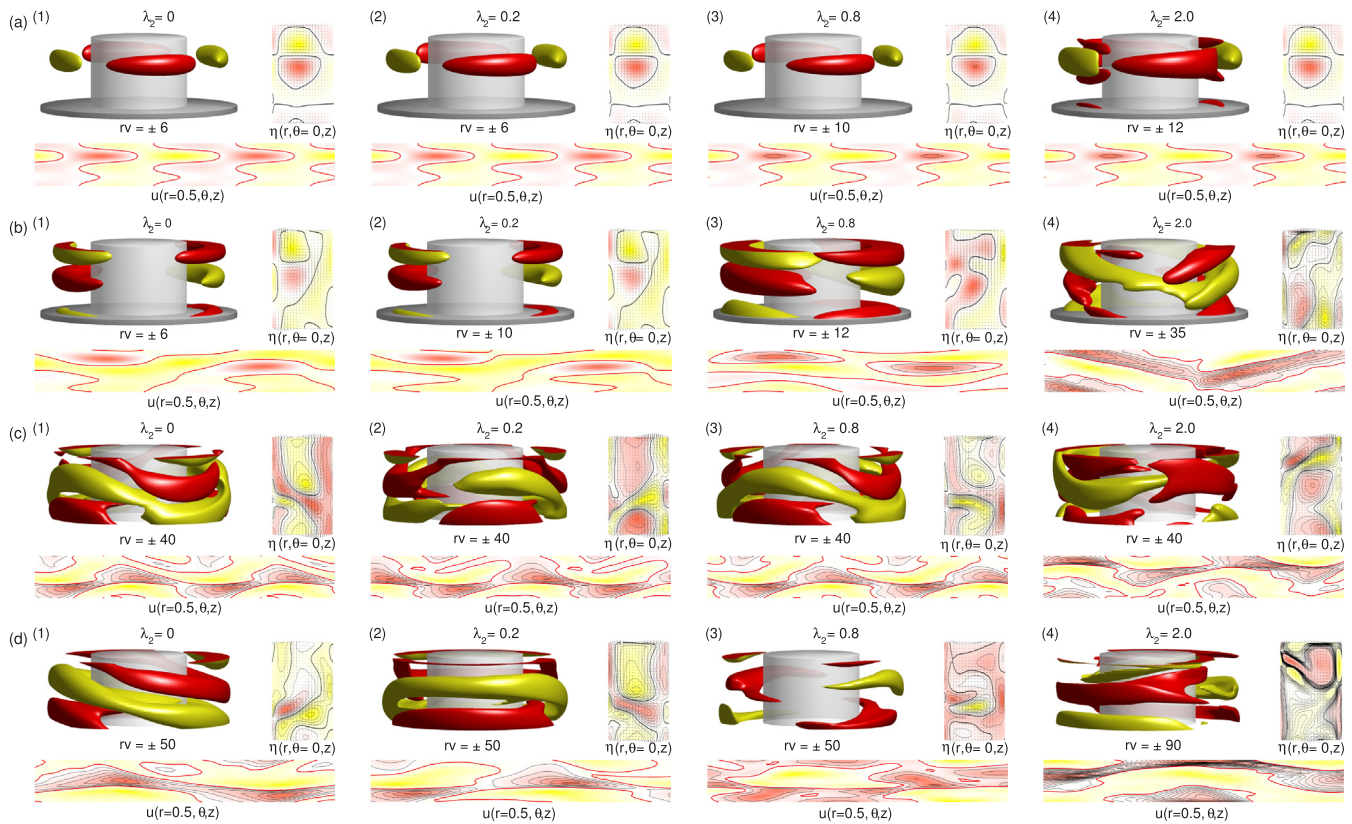


Fig. 11. Flow visualizations for  $Re_0 = -100$ . As Fig. 10 but for  $Re_0 = -100$ .

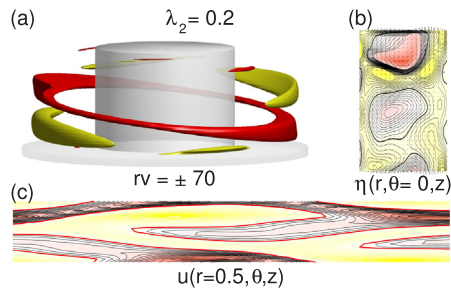


Fig. 12. Flow visualizations for  $Re_i = 600$  and  $Re_0 = 0$ . As Fig. 10 but for  $Re_i = 600$  and  $Re_0 = 0$ .

rotation frequency of the field.

Moreover, physically, particle–particle interaction, agglomeration and the chain formation result in modifications of the spatio-temporal structure of the flow. For counter-rotating cylinders the radial position at which the axial and azimuthal averaged velocity vanishes,  $\langle v(r) \rangle_{\theta, z} = 0$ , depends on the amplitude of the transport coefficient  $\lambda_2$  and thus on the agglomeration on particles. For any field configuration, from small to moderate  $Re_i$  it is mainly shifted towards the inner cylinder, while at larger  $Re_i$  it remains almost constant and slightly move outwards for large values  $\lambda_2$ .

Studying the relative energy amount  $E_{kin}/E_{cf}$ , the ratio between cross-flow  $E_{cf}$  and kinetic energy  $E_{kin}$ , we detected mainly different behavior for pure axial or transversal and oblique magnetic fields. With increasing of  $\lambda_2$  this ratio typically decreases for pure field configuration (axial and transversal) and increases in oblique field configuration, respectively. The fact that the ratio becomes largest in oblique field and large  $\lambda_2$  (as already observed before) can be traced down to the additional mode stimulation  $m = \pm 1$  in such a field [17,32], which also enter in the terms describing elongational flow. However their relative contribution has more weight at low and moderate Reynolds numbers.

Physically speaking this means the stronger the driving forces of the flow are, the less relevant are internal microscopic variations (at least as long they are relatively small). All over this suggests that particle–particle interaction and the chain formed by the flow of the fluid are more significantly influenced due to the increasing magnetic-field strength and in particular applied field direction [17,12].

Consider constant magnetic field and variation either inner cylinder rotation,  $Re_i$ , and/or transport coefficient,  $\lambda_2$ , describing elongational flow, our studies qualitative prove/confirm the field driven agglomeration, first experimental detected by Storozhenko et al. [9].

Consider finite transport coefficient  $\lambda_2$  we find the torque not to have a ‘simple’ relation/proportion with increasing the inner cylinder rotation, i.e.  $Re_i$ . One indication is the slope of the torque versus  $Re_i$ . If the ferrofluid particles would contribute independently to the torque, this slope should increase more or less linearly. In fact, the variation in torque  $\Delta G_{\lambda_2}$  shows an unexpected behavior in the torque. To be concrete, with consider larger values  $\lambda_2$  we detected the torque with increasing  $Re_i$  initially to increase, followed by a decrease and finally significant increase again. The range of decrease depend on considered  $\lambda_2$ ; the larger  $\lambda_2$  the larger the decrease. This holds for A and T field configuration in general. For O field configuration the same applies at small values  $\lambda_2$ , while for larger no decrease, only a decrease in slope can be observed. Natural explanation is that at low values  $Re_i$  the effect of aggregation, the forming of long chains play a minor role, but becomes important, at least noticeable for larger  $Re_i$ . This fact is most pronounced the larger the considered value  $\lambda_2$ .

Finally we detected variation in either the axial position of vortex centers and azimuthal zero flow which are forced due to agglomeration effects. Here crucial is the fact that for oblique field the vortex center first move outwards before it move inwards again with increasing  $\lambda_2$  while in other field configuration it shows an almost monotonical outward movement. Physically explanation can be found in the different dominant mode amplitude  $m = 1$  (see Table 1), based non-linear interaction of axial and transverse field which stimulate additional

(non-symmetric)  $m = \pm 1$  modes [17,32]. These additional stimulated helical modes strengthen the azimuthal ( $\theta$ ) flow components, in particular in the outer region. As having larger transport coefficient  $\lambda_2$  means stronger agglomeration/aggregation and/or larger ferrofluid chains this regions can be seen as slug flow and thus ‘push’ the vortex center inwards again.

This behavior applies similar for outer cylinder at rest and counter-rotating cylinders. Moreover in the case of counter-rotating cylinders either for transverse and oblique field (Fig. 9(b)) one sees a stagnation at a specific radial position.

Key attraction for the use of ferrofluids is obviously their possibility to have inter-particle interaction due to modification of their microscopic composition or due changing an applied magnetic field. This makes them a very interesting model substance for the study of the influence of inter-particle interaction on the rheological behavior of suspensions and the connection between the microstructure forced by inter-particle interaction and the macroscopic flow properties.

Given that the Taylor-Couette system provides very good conditions for well controlled experiments on the behavior of vortices, we hope that our results generate enough interest to address further experimental and numerical studies focused on agglomeration and chain formation in ferrofluids considered by elongational effect. In fact the here considered field strength  $s_x, s_z = 0.6$  equal to  $H = 41.8$  [kA/m] are easy accessible in experimental setups and the detected radial variation in the vortex center is so large that it should be also detectable in finite size systems, probably with minor amplitude due to the always present Ekman vortices in the bulk.

## Acknowledgments

S.A. is a Serra Hünter Fellow.

## References

- [1] G.I. Taylor, Stability of a viscous liquid contained between two rotating cylinders, *Philos. Trans. R. Soc. London A* 223 (1923) 289.
- [2] S. Odenbach, H.W. Müller, On the microscopic interpretation of the coupling of the symmetric velocity gradient to the magnetization relaxation, *J. Magn. Magn. Mater.* 289 (2005) 242.
- [3] M. Reindl, S. Odenbach, Effect of axial and transverse magnetic fields on the flow behavior of ferrofluids featuring different levels of interparticle interaction, *Phys. Fluids* 23 (2011) 093102.
- [4] R.E. Rosensweig, *Ferrohydrodynamics*, Cambridge University Press, Cambridge, 1985.
- [5] H.W. Müller, M. Liu, Structure of ferrofluid dynamics, *Phys. Rev. E* 64 (2001) 061405.
- [6] P.J.W. Debye, *Polar Molecules*, Dover, New York, 1929.
- [7] M.I. Shliomis, Effective viscosity of magnetic suspensions, *Sov. Phys. JETP* 34 (1972) 1291.
- [8] M.A. Martsenyuk, Y.L. Raikher, M.I. Shliomis, On the kinetics of magnetization of ferromagnetic particle suspensions, *Sov. Phys. JETP* 38 (1974) 413.
- [9] A. Storozhenko, R. Stannarius, A.O. Tantsyura, I.A. Shabanova, Measurement of the torque on diluted ferrofluid samples in rotating magnetic fields, *J. Magn. Magn. Mater.* 431 (2016) 66.
- [10] S. Odenbach, H.W. Müller, Stationary off-equilibrium magnetization in ferrofluids under rotational and elongational flow, *Phys. Rev. Lett.* 89 (2002) 037202.
- [11] S. Altmeyer, J. Lopez, Y. Do, Effect of elongational flow on ferrofluids under a magnetic field, *Phys. Rev. E* 88 (2013) 013003.
- [12] S. Altmeyer, A. Leschhorn, C. Hoffmann, M. Lücke, Elongational flow effects on the vortex growth out of Couette flow in ferrofluids, *Phys. Rev. E* 87 (2013) 053010.
- [13] P. Langevin, Magnétisme et théorie des électrons, *Ann. Chem. Phys.* 5 (1905) 70.
- [14] J. Embs, H.W. Müller, C. Wagner, K. Knorr, M. Lücke, Measuring the rotational viscosity of ferrofluids without shear flow, *Phys. Rev. E* 61 (2000) R2196.
- [15] M. Niklas, Influence of magnetic fields on Taylor vortex formation in magnetic fluids, *Z. Phys. B* 68 (1987) 493.
- [16] M. Niklas, H. Müller-Krumbhaar, M. Lücke, Taylor-vortex flow of ferrofluids in the presence of general magnetic fields, *J. Magn. Magn. Mater.* 81 (1989) 29.
- [17] S. Altmeyer, C. Hoffmann, A. Leschhorn, M. Lücke, Influence of homogeneous magnetic fields on the flow of a ferrofluid in the Taylor-Couette system, *Phys. Rev. E* 82 (2010) 016321.
- [18] S. Altmeyer, J. Lopez, Y. Do, Influence of an inhomogeneous internal magnetic field on the flow dynamics of ferrofluid between differentially rotating cylinders, *Phys. Rev. E* 85 (2012) 066314.
- [19] O. Ambacher, S. Odenbach, K. Stierstadt, Rotational viscosity in ferrofluids, *Z. Phys. B* 86 (1992) 29.
- [20] J. Singh, R. Bajaj, Couette flow in ferrofluids with magnetic field, *J. Magn. Magn. Mater.* 294 (2005) 53.
- [21] J. Singh, R. Bajaj, Stability of nonaxisymmetric ferrofluid flow in rotating cylinders with magnetic field, *Int. J. Math. Math. Sci.* (2005) 3727.
- [22] M. Reindl, S. Odenbach, Influence of a homogeneous axial magnetic field on Taylor-Couette flow of ferrofluids with low particle-particle interaction, *Expts. Fluids* 50 (2011) 375.
- [23] B. Eckhardt, S. Grossmann, D. Lohse, Torque scaling in turbulent Taylor-Couette flow between independently rotating cylinders, *J. Fluid Mech.* 581 (2007) 221.
- [24] H.J. Brauckmann, B. Eckhardt, Intermittent boundary layers and torque maxima in Taylor-Couette flow, *Phys. Rev. E* 87 (2013) 033004.
- [25] S. Altmeyer, C. Hoffmann, Secondary bifurcation of mixed-cross-spirals connecting travelling wave solutions, *New J. Phys.* 12 (2010) 113035.
- [26] A. Leschhorn, M. Lücke, C. Hoffmann, S. Altmeyer, Stability of circular Couette flow of a ferrofluid in an axial magnetic field: influence of polydispersity, *Phys. Rev. E* 79 (2009) 036308.
- [27] M. Hassan, A. Zeeshan, A. Majeed, R. Ellahi, Particle shape effects on ferrofluids flow and heat transfer under influence of low oscillating magnetic field, *J. Magn. Magn. Mater.* 443 (2017) 36.
- [28] R. Ellahi, M.H. Tariq, M. Hassan, K. Vafai, On boundary layer nano-ferrofluid flow under the influence of low oscillating stretchable rotating disk, *J. Mol. Liq.* 229 (2017) 339.
- [29] A. Zeeshan, A. Majeed, R. Ellahi, Effect of magnetic dipole on viscous ferro-fluid past a stretching surface with thermal radiation, *J. Mol. Liq.* 215 (2016) 549.
- [30] A. Majeed, A. Zeeshan, R. Ellahi, Unsteady ferromagnetic liquid flow and heat transfer analysis over a stretching sheet with the effect of dipole and prescribed heat flux, *J. Mol. Liq.* 223 (2016) 528.
- [31] C.J. Goh, N. Phan-Thien, J.D. Atkinson, Elongational flows of a dilute suspension of spheroidal particles, *J. Rheol.* 30 (1986) S75.
- [32] S. Altmeyer, Pattern formation and stability in magnetohydrodynamics – interaction of magnetic fields on ferrofluidic Taylor-Couette flow, *IntechOpen* 10 (5772) (2018) 80301 London.